Assessment of Groundwater Occurrence in a Typical Schist Belt Region in Osun State, Southwestern Nigeria using VES, Aeromagnetic Dataset, Remotely Sensed data, GIS, and MCDA Approaches

Olubusola Stephen Ilugbo (bussytex4peace44@gmail.com)
Lead City University https://orcid.org/0000-0002-1001-4815
Isaac Aigbedion
Ambrose Alli University
Oyamenda Kesyton Ozegin
Ambrose Alli University
Adesola Musa Bawallah
Federal University of Technology Yola: Modibbo Adama University of Technology

Research Article

Keywords: Groundwater Potential, Coefficient of Anisotropy, Lineamnet, Lineament Intersection Density, Slope, Overburden Thickness, Aquifer Resistivity

Posted Date: May 16th, 2022

DOI: https://doi.org/10.21203/rs.3.rs-1649269/v1

Abstract

This study presents modeling of groundwater potential in a Typical Schist Belt Region in Osun State, Southwestern Nigeria using Electrical Resistivity, Aeromagnetic, Remotely sensed data, and Multi-Criteria Decision Analysis (MCDA). Filtered and enhanced Landsat 8 OLI satellite imagery and Aeromagnetic lineaments were superimposed on Landsat lineaments to generate lineament intersection, which was subjected to line density in the ArcGIS environment to produce lineament intersection density. Eighty (80) Vertical Electrical Soundings (VES) using Schlumberger configuration were acquired within the study location. The manually processed VES data were subjected to a computer modeling program (Window Resist Version 1.0) to improve the manually derived geoelectric parameters. The geoelectric parameters from the VES interpretation were used to determine the second-order parameters. Integration of Electrical Resistivity, Aeromagnetic dataset, and Remotely Sensed data was subjected to Multi-Criteria Decision Analysis (MCDA) using Analytical Hierarchy Process (AHP) to model the groundwater potential of the investigated area. The finding from the groundwater potential map showed that the southern and traces in the northeastern and northwestern regions are indicative of high groundwater potential zone, while the northeastern, southeastern, southern, southwestern, and northwestern parts indicate moderate groundwater potential zone. Low groundwater potential zone was found in the southeastern and southwestern regions of the study area. Also, very low groundwater potential zone dominates the study area in the northern, northeastern, southeastern, southern, southwestern, northwestern, and central regions, which simply means that the investigated region is generally low in terms of groundwater potential. Boreholes and static water level data across the study area were used to validate the accuracy of the groundwater potential map. The prediction accuracy obtained showed that the techniques used in this study are capable of producing reliable and accurate results.

Introduction

The subsurface water formation has become the most significant and reliable supply of potable water due to the seasonal variation of rainfall and surface water (Adebiyi *et al.,* 2018, Alabi *et al.,* 2019). Groundwater is one of the worthy natural resources of the earth's surface which is used for many purposes such as domestic uses (for drinking and other house chores), agricultural purposes, irrigation, and industrialization (Olorunfemi 2008, Djamel, 2017, Joel *et al.,* 2016, Adeyeye *et al.* 2018, Ndikilar *et al.,* 2019). Groundwater resources are one of the major problems in the crystalline basement complex environment (Akintroinwa *et al.,* 2020, Bawallah *et al.,* 2021a) due to the lack of porosity of the crystalline nature of subsurface rock formation (Bawallah *et al.,* 2018a, Adebo *et al.,* 2019, Adebo *et al.,* 2022). The storativity of groundwater accumulation within the crystalline basement complex is determined by the degree and depth of weathering and fracturing of the subsurface rock (Singh *et al.,* 2013, Olorunfemi *et al.,* 2019, 2020). For an area to have high groundwater potential in a crystalline basement complex, the degree of weathering and fracturing must be very high (Ilugbo and Adebiyi 2017, Ilugbo *et al.,* 2018b, 2019, Bawallah *et al.,* 2021a). The overburden thickness of the weathered and fractured regions shows the intensity and nature of the geodynamic activities within the subsurface formation of the aquifer in the

terrain (Amadi and Olasehinde, 2010, Bawallah *et al.,* 2018b). The determination and evaluation of geologic features (such as fracture, fault, joint, and vein) are germane to a preliminary and adequate understanding of the terrain in regard to groundwater prospects (Olorunfemi *et al.,* 2020, Adebo *et al.,* 2022). Therefore, to determine an area of high groundwater potential that has high porosity and permeability with an abundant supply of water (Bawallah *et al.,* 2020b, 2021b), the abovementioned geological features (fractures, faults, joints, and veins) should be validated with boreholes data (Olorunfemi *et al.,* 2019). To have groundwater potential of higher reliability precision within a specific location, all the necessary or significant parameters from the surface (remote sensing) and subsurface (geoelectric and geologic) approaches that can influence the groundwater occurrence must be integrated (Adiat *et al.,* 2013, Ndatuwong and Yadav 2014, Ojo *et al.,* 2015). However, the integration of these parameters from both surface (remote sensing) and subsurface (geoelectric and geologic) approaches, is still a major issue that has not been effectively used within the study region, to be able to reflect the importance of these approaches. Whereas, most of the people living in Ilesha and its environs depend largely on surface water from streams and rivers as well as wells (subsurface water) for their domestic, industrial, and daily survival. This situation has not been helpful as a result of the common occurrence of abortive boreholes of extremely low yield, despite Government efforts at bringing the supply of water to the people, through the sinking of motorized boreholes and hand-pump wells which most have failed. This integration of various parameters that can influence groundwater can be achieved by using Multi-Criteria Decision Analysis (MCDA) by Rao and Briz-kishore, 1991, in addition, several researchers have also used the proposed approach for evaluating groundwater potential (Edet and Okereke, 1996, Ilugbo *et al.,* 2018c, Adebo *et al.,* 2018, Akinluyi *et al*., 2018, Oyedele 2019; Ilugbo *et al.,* 2020a, Al-Djazouli *et al.,* 2020, Tolche 2020, Bawallah *et al.,* 2021a, Akinluyi *et al.,* 2021, Kazeem *et al.,* 2022). The parameters were weights and rates based on their significance to water holding capacity, and the summation of the multiplication of each weighting and rating was used to determine the Groundwater Potential Index (GWPI) of each of the sounding point (Pietersen 2006, Saaty 2008, Shailaja *et al.,* 2018). They showed that the GWPI obtained in this process gives an accurate measurement of groundwater potential. However, apart from the fact that the assignment of weights to the parameters was largely subjective, the studies did not also account for the inconsistency that is most likely to characterize such subjective weight assignments. Therefore, this research was undertaken to integrate these parameters from both surface (remote sensing) and subsurface (geoelectric and geologic) approaches involving Multi-Criteria Decision Analysis (MCDA) using Analytical Hierarchy Process (AHP) to model the groundwater potential of the study area.

Site Description and Geology of the Study Area

Figure 1 shows the map of the study area with geographical locations observed within Latitude 7^0 30'N to 7^0 45'N and Longitude 4^0 40' E to 4^0 51E, which covers an area of 1000 Sq.Km. Towns and Villages characterized the investigated location with major and minor roads linking them together, which are also accessible through footpath in some regions where there are no major and minor roads. The study area's topography is characterized by hilly ridges and gentle steeps with topographical elevations varied from

320 to 390 m and enjoy a tropical climate with two distinct seasons comprising the rainy season (April to October) and dry season (November to March). The annual rainfall ranges from1,100 mm to 1,300 mm (NSRMEA, 1994) with monthly maximum mean temperature ranging from 30 ^{0}C to 35 ^{0}C which is documented between April and May. While the mean minimum monthly temperature ranges between 17 ^{0}C to 21 ^{0}C in December and January (Oladejo *et. al*., 2015). Osun and Mokuro are the two major rivers within the study area with their tributaries flowing across the entire area. Regionally, the investigated area falls within the Southwestern crystalline basement rock of Nigeria comprises migmatite-gness complex, metaigneous rock such as pelitic schist, quartzite, amphibolites, charnokitic rocks, older granite, and unmetamorphorsed dolerite dykes, which is made of heterogeneous compilation (Ramahan, 1976). The study area comprises three major geological formations such as amphibolites schist, granite gneiss, and quartz schist as shown in Figure 2. The study area is naturally impermeable to groundwater due to the crystalline nature of the underline rock. However, geodynamic activities within the terrain induced secondary porosity that lead to the availability of groundwater in the study area. The geodynamic activities which cause weathering depends on the underlying geology, topography, and climate factors (Palacky *et al*, 1981).

Methodology

Electrical Resistivity, Aeromagnetic dataset, Remotely Sensed Data, and Multi-Criteria Decision Analysis (MCDA) using Analytical Hierarchy Process (AHP) were engaged for the modeling of groundwater prospect around Ilesha and its environs, Osun State, Southwestern Nigeria. The acquired Landsat 8 OLI satellite imagery and DEM was acquired from the Global Land Cover Facility homepage (earthexplorer.usgs.gov.). It was enhanced and processed to generate different thematic maps such as slope and geomorphology. The Landsat imagery was filtered using an edge detection tool and subjected to linear stretching which performs edge detection filtering on the raster image. The calculation of slope in the *x* and *y* directions was used to identify areas of high slope in the input image. LINE module in PCI Geomatica environment to extract lineaments from the filtered image and imported to GIS environment for lineament corrections to generate lineament map of the research location. The aeromagnetic data was obtained from Nigerian Geological Survey Agency (NGSA), while the data were gridded using the minimum curvature gridding method with 500 m cell size, to produce total magnetic intensity map. 3D Euler deconvolution data was used in determining the locations and depths of the geologic sources, using the structural indexes of 1.0 and 2.0. The structural index (SI = 1.0 and 2.0) were imported to the ArcGIS 10.5 environment. The Exported structural index was georeferenced and digitized to generate an aeromagnetic lineament map to show the significance of aeromagnetic geological structures in lineament analysis and mapping for groundwater occurrence. The lineaments generated were used to determine the lineament density using the line density tool in the ArcGIS 10.5 environment. The lineaments extracted from Landsat imagery and aeromagnetic dataset were superimposed to determine lineament intersection and subjected to line density in the Geographical information system (GIS) environment to generate the lineament intersection density. Eighty (80) Vertical Electrical Sounding (VES) using Schlumberger configuration were acquired within the study location (Figure 3). This involves

sending alternating current (AC) into the ground utilizing two electrodes, C_1 and C_2. The potential difference between the two electrodes is measured by another pair of electrodes, P_1 and P_2 at the surface which was within the current electrodes (Telford *et al.*, 1990). That Data was acquired using a Pasi resistivity meter. The VES data were first processed manually using the conventional method and subsequently subjected to a computer modeling program (Window Resist Version 1.0) to improve the manually derived geoelectric parameters. The geoelectric parameters from the VES interpretation were used to determine the second-order parameters and used to model necessary maps. Integration of Electrical Resistivity, Aeromagnetic, and Remotely Sensed data were subjected to MCDA using Analytical Hierarchy Process (AHP) to model the groundwater potential of the investigated area. The Analytical Hierarchy Process was used to prepare the pair-wise comparisons and ratings of the parameters (Table 1); considering two parameters at a time and scoring each parameter per its relevance to groundwater occurrence. Eight (8) parameter pair-wise comparisons were considered in this study for groundwater occurrence using pair-wise comparisons techniques (Kardi, 2006, Adiat *et al.,* 2013). The number of comparisons for n numbers of factors must be added which is given by

$$\text{Number of comparison} = \frac{n(n-1)}{2} \quad \ldots\ldots\ldots\ldots\ldots\ldots\ldots\ldots\ldots\ldots\ldots\ldots\ldots\ldots \ldots\text{i}$$

where n = number of parameters being considered.

Table 1: scale for pairwise comparisons (Kardi, 2006, Adiat *et al.,* 2013)

Score	Judgment	Explanation
1	Equally	Two factors contribute equally to the objective
3	Slightly favour	Slightly favour one attribute over another
5	Strongly favour	Strongly favour one attribute over another
7	very strongly	Strongly favour one attribute with demonstrated importance over another
9	Extremely	Evidence favouring one attribute over another is one of the highest possible order of affirmation
2, 4, 6, 8	Intermediate	The intermediate values are used when compromise is needed

The pairwise comparisons were used to generate the pairwise comparison matrix for groundwater potential (Table 2). Figure 4a to f show the respective pairwise comparisons of the Coefficient of

Anisotropy (CA)/Overburden Thickness (OT), Coefficient of Anisotropy (CA /Lineament Intersections Density (LID), Coefficient of Anisotropy (CA)/Aquifer Resistivity (AR), Coefficient of Anisotropy (CA)/Aquifer Thickness (AT), Coefficient of Anisotropy (CA)/Slope (S), and Coefficient of Anisotropy (CA)/Geomorphology (Geom.) in accordance to their respective significance on groundwater evaluation. From the Figures, CA is slightly favoured over OT, LID, AR, AT, S, and Geom hence number “3” is marked (in yellow colour) on the left side of “1” for the two cases. Similarly, CA is strongly favoured over geology (G) as shown in Figure 4g, hence number “5” is marked on the left side of “1”. Figure 4h to m shows the pairwise comparisons of OT/LID, OT/AR, OT/AT, OT/S, OT/Geom, and OT/G. From the figures, OT is slightly more favoured over LID, AR, AT, S, and Geom. while it is strongly more favoured than G, hence “3” and “5” are marked on the left side of “1” for their respective comparisons. Figure 4n to r shows the pairwise comparisons of LID/AR, LID/AT, LID/S, LID/Geom., and LID/G. From the figures LID is slightly more favoured than AR, AT, S, and Geom. while it is strongly more favoured than G, hence “3” and “5” are marked on the left side of “1” for their respective comparisons. Figure 4s to v shows the pairwise comparisons of AR/AT, AR/S, AR/Geom., and AT/G. From the figures AR is slightly more favoured than AT, S, and Geom. while it is strongly more favoured than G, hence “3” and “5” are marked on the left side of “1” for their respective comparisons. Figure 4w to y shows the pairwise comparisons of AT/S, AT/Geom., and AT/G. From the figures AT is slightly more favoured than S, and Geom. while it is strongly more favoured than G, hence “3” and “5” are marked on the left side of “1” for their respective comparisons. Figure 4z to aa shows the pairwise comparisons of S/Geom., and S/G. From the figures S is equal to Geom. while it is strongly more favoured than G, hence “1” and “5” are marked on the left side of “1” for their respective comparisons.

Finally, Figure 4ab shows that Geom. is strongly favoured than G, and hence “5” is marked on the left side of “1”. A Pairwise comparison matrix was formed using the described above pairwise comparisons.

Table 2: Pairwise comparison matrix for Groundwater Potential

		A	B	C	D	E	F	G	H
CA	A	1	3	3	3	3	3	3	5
OT	B	1/3	1	3	3	3	3	3	5
LID	C	1/3/	1/3	1	3	3	3	3	5
AR	D	1/3	1/3	1/3	1	3	3	3	5
AT	E	1/3	1/3	1/3	1/3	1	3	3	5
Slope	F	1/3	1/3	1/3	1/3	1/3	1	1	5
Geom.	G	1/3	1/3	1/3	1/3	1/3	1	1	5
G	H	1/5	1/5	1/5	1/5	1/5	1/5	1/5	1
TOTAL		3.2	5.87	8.53	11.2	13.87	17.2	17.2	36

Calculation of Multi-criteria Evaluation Techniques (MCDA)

MCDA techniques were used to assign weight to each parameter (Edet and Okereke, 1996, Malczewski, 1999), which allows model layers to be weighted by their significant influence (Ilugbo *et al.,* 2018c, Adebo *et al.,* 2018). This was accomplished by adding the value of each column of the pairwise comparison matrix (Table 2) dividing each value in the matrix by its column total, and finally, calculating the average value in each of the normalized matrices (Table 3). These averages give an estimate of the relative weights of the parameter being compared (Akinluyi *et al*., 2018, Al-Djazouli *et al.,* 2020, Tolche 2020, Akinluyi *et al.,* 2021, Kazeem *et al.,* 2022). The final weight of the parameters was computing by adding all the values along each row. The relative weights of the criteria are shown in Table 3.

Table 3: Calculation of the Criteria Weights

	CA (j=1)	OT (j=2)	LID (J=3)	AR (j=4)	AT (j=5)	Slope (j=6)	Geom. (j=7)	G (j=8)	ΣWij
CA (i=1)	0.31	0.51	0.35	0.27	0.22	0.17	0.17	0.14	2.14
OT (i=2)	0.10	0.17	0.35	0.27	0.22	0.17	0.17	0.14	1.59
LID (i=3)	0.10	0.06	0.12	0.27	0.22	0.17	0.17	0.14	1.25
AR (i=4)	0.10	0.06	0.04	0.09	0.22	0.17	0.17	0.14	0.99
AT (i=5)	0.10	0.06	0.04	0.03	0.07	0.17	0.17	0.14	0.78
Slope (i=6)	0.10	0.06	0.04	0.03	0.02	0.06	0.06	0.14	0.51
Geom. (i=7)	0.10	0.06	0.04	0.03	0.02	0.06	0.06	0.14	0.51
G (i=8)	0.06	0.03	0.02	0.02	0.01	0.01	0.01	0.03	0.19
Σj	1	1	1	1	1	1	1	1	ΣWij/Σj = 1

Estimation of the Groundwater Potential Index (GWPI)

The following mathematical expressions were used to generate the final GWPI.

Mathematically, this can be defined as:

GWPI = f (CA, OT, LID, AR, AT, S, Geom, and G) ……2

Where, GWPI is groundwater Potential Index, CA is Coefficient of Anisotropy, OT is Overburden Thickness, LID is Lineament Intersections Density, AR is Aquifer Resistivity, AT is Aquifer Thickness, S is Slope,

Geom. is Geomorphology, and G is geological.

The groundwater potential map value, thus derived is given by the equation:

GWPI = $\sum$WiCVi ; with $\sum$Wi = 1; ……3

Where GWP is the groundwater potential Index, Wi is the probability value of each thematic map, and CVi is the individual capability value to potentiality influence. The final Map was validated using hydrogeologic data obtained from existing boreholes and wells across the study area (Figure 5). The borehole data were obtained from Drilling Log under FADB RWSS (Rural Water Sanitation Supply) in OSUN STATE. The instrument used for static water level includes the following; field notebook, Global Positioning System (GPS), and measuring tape.

Results And Discussion

Remote Sensing

Figure 6a illustrates the slope of the study area which was calculated in degrees in both vector and raster forms, which ranged from 0^o to 39.62^o with topographic slope classes of nearly level. The regions of high surface gradient (slope) which vary from 10.41^o to 39.62^o are indicative of low groundwater prospecting due to high runoff of water most especially from rainfall (Oyedele 2019; Ilugbo *et al.,* 2020a, Al-Djazouli *et al.,* 2020, Akinluyi *et al,.* 2021),. The areas with values ranging from 3.57^o to 10.41^o have little infiltration of water which exhibits moderate groundwater prospects. Whereas, areas of low surface gradient (slope) that vary from 0^o to 3.57^o are indicative of high groundwater prospect, which allows a high degree of water infiltration into the subsurface. Geomorphology reflects different categories of landforms and subsurface geological features which are favourable to groundwater accumulation (Talabi and Tijani 2011, Waikar and Aditya, 2014). The study area was classified into five categories to their significance to groundwater occurrence (Figure 6b). Alluvium and pediplain have better prospects for groundwater development compared to pediment (Waikar and Aditya 2014, Oyedele 2019, Ilugbo *et al.,* 2020a, Al-Djazouli *et al.,* 2020, Akinluyi *et al.,* 2021). Valley fills and hills and ridges have low groundwater prospect due to the low degree of infiltration of water with high runoff. Figure 6c shows the lineaments map extracted from the Landsat TM imagery to delineate regions with high occurrence for groundwater prospects. Elimination and isolation techniques were carried out for the correctness of the lineament map to determine those that are not hydro-geological significant. The eastern, northeastern, and small traces of lineaments at the southwestern parts are indicative of geological structures such as fracture, fault, cavity, and joint which has high groundwater prospect (Bayowa *et al.,* 2014, Ojo *et al.,* 2015, Ilugbo and Adebityi 2017), whereas the remaining parts of the region have low concentration of lineaments which indicate low groundwater prospect. The lineaments trend approximately NE-SW and NW – SE directions. The lineament density was computed based on the number of lineaments per unit area (Kg/Kg^2) of the grid, for a quick graphical evaluation of the lineament density values of the area (Figure 6d). The lineament density showed four groundwater prospect zones distributed as patches in the study location.

Regions with high lineament density marked red at the northeastern and southeastern parts ranging from 3.00 to 4.00 Kg/Kg^2 indicatives of a good prospect for groundwater exploration (Bayowa *et al.,* 2014, Al-Djazouli *et al.,* 2020, Akinluyi *et al.,* 2021,). Lineament density outlined in yellow and blue colours in the northern, northeastern, eastern, southeastern, and traces at the southwestern parts of the study area show low to moderate groundwater prospect, while the majority of the investigated area represents very low hydro-lineament density indicative of very low prospect for groundwater potential.

Aeromagnetic Data

Aeromagnetic Lineament Map

The structural index (SI = 1.0 and 2.0) produced was exported from Oasis Montaj (GEOSOFT packages) and imported into the ArcGIS environment (Figure 7a). The imported Structural Index was georeferenced and digitized to generate an aeromagnetic lineament map (Figure 7b) to show the significance of aeromagnetic geological structures in lineament analysis and mapping to determine subsurface geological fissures such as fault, joint, fracture, and cavity within the area of interest (Djamel 2017, Ilugbo *et al.,* 2020b). Fifty-eight (58) lineaments were delineated from the aeromagnetic lineaments map which shows one major set of lineaments oriented towards the NE-SW direction which are related to tectonic activity vis-à-vis faults, fracture, and joints in the area of interest (Megwara and Udensi 2013, Ogunmola *et al.,* 2014). The majority of the lineaments are concentrated in the southwestern and northwestern parts of the area, whereas, an area with high concentration of lineaments has a better prospect for groundwater. Aeromagnetic lineament density related to basement complex terrain is mostly used in groundwater development investigation (Ilugbo and Ozegin, 2018). Figure 7c shows the aeromagnetic lineament density map which delineates four various hydrogeological prospect regions distributed as patches within the study location. Regions with high lineaments density has better prospect for groundwater development (Ilugbo *et al.,* 2020a, Tolche 2020, Akinluyi *et al,.* 2021). These were observed at the eastern and southwestern parts of the area as groundwater occurs within faults and fractures in the basement rocks. Moderate and low lineament density was found in most parts of the study area, indicative of low to moderate groundwater development. The study has a high percentage of very low lineament density which is indicative of very low groundwater prospects.

Lineament Intersection and Lineaments Intersection Density Map

Figure 8a displays a lineaments intersection map including Landsat lineaments and Aeromagnetic lineaments within the study area. Lineament intersection is a point of major weakness (node points) between two or more lineaments (Bayowa *et al.,* 2014). The map shows that the lineament intersections are comparatively concentrated in the northeastern regions of the area; whereas, the remaining parts of the area have little or no lineament intersection indicates of a low groundwater prospect. Area with high lineaments intersection concentration suggests high prospect for groundwater potential (Akinluyi *et al.,* 2021). The lineaments intersection shows that the fractures are tending towards the NE direction, indicating groundwater potential zone and hence better prospect for groundwater availability

Figure 8b displays a lineament intersection density map of the investigated area. lineament intersection density determines the cluster of geological features within an area (Bayowa *et al.,* 2014, Akinluyi *et al.,* 2021). The highest region of lineament intersection density contour models has a better prospect for groundwater development excluding the ridges and valley hills areas (Ilugbo and Adebiyi, 2017). The map identifies four various hydrogeological prospect areas which were classified as very low, low, moderate, and high lineament intersection density. The regions with high and moderate lineament intersection density (outlined red and yellow colour respectively) were observed around northeastern, eastern, southeastern, and traces at the western parts of the investigated area. This indicates that the region has moderate to high groundwater prospect. Low lineaments intersection density (outlined blue colour) was also found around northeastern, eastern, southeastern, and traces at the western parts of the investigated area indicative of low groundwater prospect, while eighty percent (80%) of the area were characterized with very low lineament intersection density indicating very low prospect for groundwater development (Bayowa *et al.,* 2014, Ilugbo and Adebiyi 2017).

Vertical Electrical Sounding

Data acquired from vertical electrical sounding (VES) using Schlumberger and Wenner depth soundings were interpreted, first using manual partial curve matching techniques, and subsequently subjected to computer iterative modeling. Figure 15 shows typical iterated VES data curves and the estimated geoelectric parameters.

Sounding Curves and Aquifer types

In the study area, eight (8) curve types were identified, these are A, H, QH, HA, KH, KHA, KQH, and KHK (Figure 9). KH curve-type has the highest percentage (31.25%) of occurrence, while the KHA curve-type has the least percentage of 1.25%.

Geoelectric Maps

Aquifer Resistivity Map

Figure 10a exhibits the aquifer resistivity map of the investigated area which is categorized into low, moderate, and high. Low aquifer resistivity was found at Asegbo, Agbao, Ileromaja, and Ilesha indicating low groundwater prospects. The following localities were classified as moderate aquifer resistivity; Isaobi, Araromi, Oja Oko, Iwori, Irefon, Iyere, Aye, Imosan Ile, Aba Fadugba, and Eyinla exhibiting moderate groundwater prospect. However, high aquifer resistivity was established at localities such as Oko Asa, Ilotin, Olorunda, Akola, Isotun, Ijano, Afo, Borakodo, Ilosi, Oke Agbe, and Oloyin suggesting high groundwater prospects. Figure 10b displays the aquifer thickness map of the study area which was classified into low, moderate, and high. The low aquifer thickness was observed at some localities such as Oke Agbe, Eyinta, Aba Fadugba, Igila, Olorombo, Ijano, Imosan Ile, Oloyin, Ibodi, Shasha, and Iloki suggesting low rate of groundwater accumulation within the regions. The high percentage of the investigated area was considered to have moderate aquifer thickness at Iwori, Ita Osan, Ilotin, Akola,

Olorunda, Borakodo, Loroyun, Oko Osin, Isotun, Irefon, Iyere, Agbao, and Ileromaja indicating moderate rate of groundwater accumulation within the regions. The high aquifer thickness regions suggest a significant amount of groundwater accumulation within the area, especially, if the formation has high permeability. However, some portions of the high aquifer thickness correlate with an area of high aquifer resistivity (permeable media) showing high prospect for groundwater occurrence in northeastern, northwestern, and small portions of southeastern and southwestern parts of the study area. The overburden thickness of the investigated area was produced using the summation of all the depths of topsoil, weathered layer, and fractured basement before the fresh basement of Vertical Electrical Sounding (VES) points (Figure 10c). Overburden thickness is the loose materials before the fresh basement. The overburden thickness varies from 2.9 to 89 m. The regions with high overburden thickness (above 30 m) in northeastern and small portions in the southeastern, southwestern, northwestern, and the central part correlate with areas of high aquifer resistivity and aquifer thickness. These regions have a good prospects for groundwater occurrence, particularly when underlain by weathered basement and fractured basement (Ilugbo *et al.,* 2018c, Adebo *et al.,* 2018, Bawallah *et al.,* 2021a, Kazeem *et al.,* 2022). The regions with moderate overburden thickness occupied more than 75% of the study area in northern, northeastern, eastern, southeastern, southern, southwestern, northwestern, and central parts indicating moderate prospect for groundwater accumulation. The regions with low overburden thickness (less than 15 m) were observed in southwestern and southwestern parts, also correlate with areas of low aquifer resistivity and aquifer thickness indicating low prospect for groundwater development.

Dar Zarrouk Parameters for Groundwater Characteristics

Dar-Zarrouk parameters were generated from the geoelectric parameters using the necessary formulae. Figure 11a displays total longitudinal conductance that varied from 0.0041 – 0.89 Ω^{-1}. The significant use of the Dar Zarrouk parameter is to disintegrate the differences in total thickness of low resistivity materials (Bawallah *et al.,* 2021a, Kazeem *et al.,* 2022). The high longitudinal conductance was observed around Aba Fadugba, Shasha, and Agbao in the southwestern part of the investigated area, while moderate longitudinal conductance was found around Iyere, Aye, Oloyin, Oko Asa, and Araromi in the northeastern, southwestern, northwestern, and small portions at the southeastern region of the area. The low total longitudinal conductance covered 80% of the study area in northern, northeastern, eastern, southeastern, southern, southwestern, western, northwestern, and central parts of the areas. The total transverse resistance varied from 483.18 – 50,000 Ωm, which gives useful information about the thickness and resistivity of the area (Figure 11b). The total transverse resistance was categorized into low, moderate, and high. The low transverse resistance was established in southwestern and small portions across the study area, while the moderate total transverse resistance was observed in the northern, northwestern, southwestern, and small closures at the eastern, northeastern, and southeastern. The high total transverse resistance was found in the northeastern, eastern, southeastern, and small portions of the southwestern parts of the investigated area. The average longitudinal resistivity calculated from sounding curves helps in calculating the total depth H to the high resistivity bedrock and the average transverse resistivity showed that it is more than the average longitudinal resistivity. This

indicates that the true resistivity normal to the plane of structural features is greater than the true resistivity parallel to the plane of structural features (Ilugbo *et al.,* 2018b, Adebo *et al.,* 2018, Kazeem *et al.,* 2022). Based on the estimation, the coefficient of anisotropy was determined from the square root of average longitudinal resistivity and the average transverse resistivity with values ranging from 0.01 – 1.87 which exhibits the degree of variation of anisotropy in rock formation (Figure 11c). The regions with high coefficient of anisotropy values ranged from 1.45 – 1.87 in the southeastern, southern, central, and a portion of the northwestern. These show that the degree of weathering and fracturing of the rock formation must have extended in all directions, which had high groundwater accumulation capacity resulting in higher porosity (Ojo *et al.,* 2015, Olorunfemi *et al.,* 2019, Bawallah *et al.,* 2021a). Whereas, unidirectional structures (Fracture/fault) have low degree of groundwater holding capacity due to low coefficient of anisotropy which was observed in the northern, northeastern, eastern, southwestern, northwestern and small portion of the southeastern parts of the study area, which shows the presence of macro-anisotropy in the geoelectric structures in the area (Adebo *et al.,* 2018, Bawallah *et al.,* 2021a, Kazeem *et al.,* 2022). The moderate coefficient of anisotropy was observed in the southern, southeastern, southwestern, central part, northeastern, and northwestern regions of the study area indicating moderate prospect for groundwater accumulation.

Modeling of Groundwater potential

The groundwater potential rate (R) gives the ranges of groundwater storage potentiality within each parameter (Edet and Okereke, 1996, Pietersen 2006, Saaty 2008, Adiat *et al.,* 2013, Shailaja *et al.,* 2018, Adebo *et al.,* 2018, Akinluyi *et al*., 2018, Oyedele 2019; Ilugbo *et al.,* 2020a, Al-Djazouli *et al.,* 2020, Tolche 2020, Bawallah *et al.,* 2021a, Akinluyi *et al,.* 2021, Kazeem *et al.,* 2022). Each parameter was classified and rated. However, since resistivity and thickness do not have the same unit, a unified scaling technique was adopted in rating these parameters according to their degree of influence on groundwater occurrence (Pietersen 2006, Saaty 2008, Adiat *et al.,* 2013, Shailaja *et al.,* 2018, Adebo *et al.,* 2018, Ilugbo *et al.,* 2020a, Tolche 2020, Kazeem *et al.,* 2022). Different types of lithology with different resistivity and thickness ranges will have different groundwater prospects (Pietersen 2006, Saaty 2008, Shailaja *et al.,* 2018),. Therefore, different ranges of values or features should have a different rating (R) on a scale according to their importance in accumulating groundwater (Adiat *et al.,* 2013). In this study, each parameter has been scored on the 1–5 scale in the ascending order of hydrogeologic significance. However, the resistivity range of any given rock type is wide and overlaps with other rock types. Therefore, different types of lithology may have the same resistivity values. The classifications and ratings of each parameter are shown in Table 4. The weighted linear combination (WLC) is applied according to the following equation to estimate the GWPI. This technique is usually specified in terms of normalized weightings (w) for each criterion as well as rating scores (R) for all classes relative to each of the criteria. The final GWPI obtained for all the locations.

Table 4: Probability rating (R) for classes of the parameters

Influencing Factors	Category (Classes)	Potentiality for Groundwater Storage	Rating (R)	Normalized Weight (W)
Coefficient of Anisotropy (CA)	0.01 – 1.15	Low	2	2.14
	1.15 – 1.45	Moderate	3	
	1.45 - 1.87	High	4	
Overburden Thickness (OT)	2.9 – 15.0	Low	2	1.59
	15.0 – 30.0	Moderate	3	
	30.0 – 89	High	4	
Lineament Intersections Density (LID)	0 – 1.25	Very low	1	1.25
	1.25 – 2.50	Low	2	
	2.50 – 3.75	Moderate	3	
	3.75 – 5.00	High	4	
Aquifer Resistivity (AR)	31 – 100	Low	2	0.99
	100 – 150	Moderate	3	
	150 - 298	High	4	
Aquifer Thickness (AT)	0.9 – 15	Low	2	0.78
	15 – 25	Moderate	3	
	25 – 59.8	High	4	
Slope	0 – 3.57	Very Low	1	0.51
	3.57 – 6.53	Low	2	
	6.53 – 10.41	Moderate	3	
	10.41 – 16.78	High	4	
	16.78 – 39.62	Very High	5	
Geomorphology	Valley Hills	Very High	5	0.51
	Alluvium	High	4	
	Pediplain	Moderate	3	
	Pediment	Low	2	
	Hills and Ridges	Very Low	1	
Geology (G)	Amphibolit	Low	2	0.06

	Schist	Moderate	3
	Granite Gneiss	Moderate	3
	Quartz Schist		

The groundwater potential index obtained for each location was interpolated using inverse distance weighting (IDW) techniques in ArcGIS 10.1 to produce the groundwater potential map shown in Figure 12. It was observed from the groundwater potential map, that the southern and traces at the northeastern and northwestern regions around Ijona, Olorunda, and Iyemogun are indicative of high groundwater potential zone, while the regions around Oke Osin, Oke Asa, Ejiro, Araromi, Iyere, Ilosi, and Shasha of the study area indicates moderate groundwater potential zone. Low groundwater potential zone was found at the Eyinta, Imosan Ile, Iloki, Olorombo, and Igila of the study area. Also, very low groundwater potential zone dominates the study area in the northern, northeastern, southeastern, southern, southwestern, northwestern, and central regions, which simply means that the investigated region is generally low in terms of groundwater potential.

Validation of Groundwater Potential Map

Borehole Drilled and static water levels across the investigated area were used to validate the integration results of VES, aeromagnetic dataset, satellite remotely sensed data, MCDA, and groundwater potential map. Figure 13 shows the validation map in which the locations and names of the boreholes and static water levels are displayed. Boreholes and static water level data were superimposed on the groundwater potential map; the expected yield of its location on the groundwater potential map was compared with the actual yield of each borehole and static water level data. Tables 6 and 7 showed the coincidence (agreement) between the actual and the expected yields.

Based on these tables, the accuracy of the prediction is estimated as follows:

The accuracy of Borehole data

Total number of boreholes = 20

Number of boreholes where the expected and actual yield coincide = 20

Number of boreholes where the expected and actual yield did not coincide = 0

Accuracy of borehole data on the groundwater potential map is = 20/20 x 100 = 100%

The accuracy of well data (Static water level)

Total number of wells = 30

Number of wells where the expected and actual yield coincide = 27

Number of wells where the expected and actual yield did not coincide = 3

Accuracy of well data on the groundwater potential map is = 27/30 x 100 = 90%

Borehole and well data give 100% and 90% accuracy

To determine the overall accuracy for both boreholes and well data, the accuracy of the prediction is estimated as follows:

Total number of boreholes = 20

Total number of wells = 30

The total for both boreholes and wells = 50

Number of boreholes and wells where the expected actual yield coincide = 47

Number of boreholes and wells where the expected actual yield did not coincides = 3

Then the accuracy of the groundwater potential for both borehole and well data is = 47/50 x 100 = 94%

The prediction accuracy obtained showed that the proposed method in this study is capable of producing accurate and reliable results.

Table 6: Validation of Borehole Data for the Groundwater Potential Map

Borehole Number	Expected Yield Description from the Groundwater Potential Map	Actual Yield from the Drilled Borehole (litres/hr)	Actual Description	Remarks
BH1	Low	662	Low	Coincide
BH2	High	3004	High	Coincide
BH3	Low	660	Low	Coincide
BH4	Moderate	817	Moderate	Coincide
BH5	High	2280	High	Coincide
BH6	Moderate	1021	Moderate	Coincide
BH7	High	2620	High	Coincide
BH8	Very Low	310	Very Low	Coincide
BH9	Low	592	Low	Coincide
BH10	Moderate	945	Moderate	Coincide
BH11	Low	721	Low	Coincide
BH12	Low	598	Low	Coincide
BH13	High	2301	High	Coincide
BH14	Low	610	Low	Coincide
BH15	Low	522	Low	Coincide
BH16	Low	611	Low	Coincide
BH17	Moderate	896	Moderate	Coincide
BH18	Moderate	992	Moderate	Coincide
BH19	Moderate	943	Moderate	Coincide
BH20	Very Low	345	Very Low	Coincide

Table 7: Validation of Wells Data for the Groundwater Potential Map

Well Numbers	Depth (m)	Static Water Level (m)	Groundwater yield Thickness (m)	Expected Yield Description from the Groundwater Potential Map	Actual Yield from the wells (m)	Remarks
W1	12.9	12	0.9	Low	Low	Coincide
W2	8.6	8.3	0.3	Low	Low	Coincide
W3	11.8	11.15	0.65	Low	Low	Coincide
W4	6.8	6	0.8	Moderate	Low	Not Coincide
W5	13	12.9	0.1	Very low	Very low	Coincide
W6	13.3	13	0.3	Very Low	Very Low	Coincide
W7	10.6	9.7	0.9	Low	Low	Coincide
W8	8.2	7.1	1.1	Moderate	Moderate	Coincide
W9	18.6	dry	dry	Very low	Very low	Coincide
W10	20.2	18.1	2.1	Moderate	Moderate	Coincide
W11	14.3	10.2	4.1	High	High	Coincide
W12	9.2	8.1	1.1	Moderate	Moderate	Coincide
W13	8.6	6.2	2.4	Moderate	High	Not Coincide
W14	9.6	8.8	0.8	Low	Low	Coincide
W15	7.9	7.4	0.5	Very Low	Very Low	Coincide
W16	8.7	6.3	2.4	Moderate	High	Not Coincide
W17	9.5	8.3	1.2	Moderate	Moderate	Coincide
W18	8.2	7.6	0.6	Low	Low	Coincide
W19	7.9	7.1	0.8	Low	Low	Coincide
W20	8.7	8.1	0.6	Low	Low	Coincide
W21	9.1	8.6	0.5	Low	Low	Coincide
W22	10.4	9.8	0.6	Low	Low	Coincide
W23	7.4	Dry	Dry	Very Low	Very Low	Coincide
W24	8.7	6.9	1.8	Moderate	Moderate	Coincide
W25	11.6	10.9	0.7	Low	Low	Coincide

W26	9.3	8.8	0.5	Low	Low	Coincide
W27	10.3	9.2	1.1	Moderate	Moderate	Coincide
W28	9.5	8.8	0.7	Low	Low	Coincide
W29	10.2	9.6	0.6	Low	Low	Coincide
W30	10.7	9.9	0.8	Low	Low	Coincide

Conclusion

This research work has been able to justify the tautology of MCDA in groundwater occurrence modeling in a Typical Schist Belt region of Ilesha and its environs, Southwestern Nigeria. The groundwater potential index obtained for each location was interpolated using inverse distance weighting (IDW) techniques to produce the groundwater potential map of the investigated area. It was observed from the groundwater potential map, that the southern and traces at Ijona, Olorunda, and Iyemogun are indicative of high groundwater potential zone, while the area around Oke Osin, Oke Asa, Ejiro, Araromi, Iyere, Ilosi, and Shasha of the study area indicates moderate groundwater potential zone. Low groundwater potential zone was found in the Eyinta, Imosan Ile, Iloki, Olorombo, and Igila regions of the study area. Also, very low groundwater potential zone dominates the study area in the northern, northeastern, southeastern, southern, southwestern, northwestern, and central regions. Boreholes and static water level acquired within the study area was used to validate the integrated results of the VES, aeromagnetic dataset. Satellite remotely sensed data, MCDA, and groundwater potential model. The prediction accuracy obtained showed that the proposed method in this study is capable of producing accurate and reliable results.

Declarations

Funding; This study did not receive any funding from governmental or non-governmental financial assistance in order to carry out this research.

Conflicts of interest; The authors declare that there is no conflict of interest

Code availability: Not applicable

Author contributions; All authors contributed to every section of this manuscript.

References

Adiat K.A.N., Nawawi M.N.M., Abdullah K. 2013. Application of Multi-Criteria Decision Analysis to Geoelectric and Geologic Parameters for Spatial Prediction of Groundwater Resources Potential and Aquifer Evaluation. Pure Appl. Geophys. 170, 453–471. Doi 10.1007/s00024-012-0501-9

Adebiyi, A.D., Ilugbo, S.O., Bamidele, O.E., Egunjobi, T., 2018. Assessment of Aquifer Vulnerability Using Multi- Criteria Decision Analysis around Akure Industrial Estate, Akure, Southwestern Nigeria. Journal of Engineering Research and Reports 3 (3), 1-13. International 23(4), 1-15.

Adebo B.A., Ilugbo S.O., Jemiriwon E.T., Ali A.K., Akinwumi A.K., Adeniken N.T. 2022. Hydrogeophysical Investigation Using Electrical Resistivity Method within Lead City University Ibadan, Oyo State, Nigeria. International Journal of Earth Sciences Knowledge and Applications, 4(1), 51-62

Adebo, B.A., Layade, G.O., Ilugbo, S.O., Hamzat, A.A., Otobrise, H.K., 2019. Mapping of Subsurface Geological Structures using Ground Magnetic and Electrical Resistivity Methods within Lead City University, Southwestern Nigeria. Kada Journal of Physics 2 (2), 64-73.

Adebo, A.B., Ilugbo, S.O., Oladetan, F.E., 2018. Modeling of Groundwater Potential Using Vertical Electrical Sounding (VES) and Multi-caterial Analysis at Omitogun Housing Estate, Akure, Southwestern Nigeria. Asian Journal of Advanced Research and Reports 1 (2), 1-11.

Adeyeye OA, Ikpokonte EA, Arabi SA (2018) GIS-based groundwater potential mapping within Dengi area, North Central Nigeria. Egypt J Remote Sens Space Sci 22:175–181. https ://doi.org/10.1016/j.ejrs.2018.04.003

Alabi, T.O., Ilugbo, S.O., Akinmoye, O.E., Ibitomi, M.A., Aigbedion, I., Adeleke, K.A., Ajanaku, B.S., 2019. Application of Electrical Resistivity and Hydrochemistry Methods for Mapping Groundwater Contamination around Okun Ilashe Island Area, Lagos State, Southwestern Nigeria, Journal of Geography, Environment and Earth Science

Al-Djazouli MO, Elmorabiti K, Rahimi A, Amellah O, Fadil OAM (2020) Delineating of groundwater potential zones based on remote sensing, GIS and analytical hierarchical process: a case of Waddai, eastern Chad. GeoJournal. https ://doi.org/10.1007/ s1070 8 020-10160 -0

Akinluyi A.O., Olorunfemi M.O., Bayowa O.G. 2021. Application of remote sensing, GIS and geophysical techniques for groundwater potential development in the crystalline basement complex of Ondo State, Southwestern Nigeria. Sustainable Water Resources Management, 7(4), 1-15. https://doi.org/10.1007/s40899-020-00486-5

Akinluyi F.O., Olorunfemi M.O., Bayowa O.G. 2018. Investigation of the influence of lineaments, lineament intersections and geology on groundwater yield in the basement complex terrain of Ondo state, Southwestern Nigeria. Appl Water Sci. https ://doi.org/10.1007/s1320 1-018-0686-x

Akintorinwa O.J., Atitebi M.O., Akinlalu A.A. 2020. Hydrogeophysical and aquifer vulnerability zonation of a typical basement complex terrain: A case study of Ododе Idanre southwestern Nigeria. Heliyon, 1-20 https://doi.org/10.1016/j.heliyon.2020.e04549

Amadi, A.N., Olasehinde, P.I. 2010. Application of Remote Sensing Techniques in Hydrogeological Mapping of parts of Bosso Area, Minna, North Central Nigeria. International Journal of the Physical Sciences, 5, 1465-1474.

Bayowa O.G., Olorunfemi M.O., Akinluyi F.O., Ademilua O.L. 2014. Integration of Hydrogeophysical and Remote Sensing data in the assessment of groundwater potential of the basement complex terrain of ekiti state, southwestern Nigeria. Ife J. Sci. 16(3).

Bawallah M.A., Adiat K.A.N., Akinlalu AA., Ilugbo S.O., Akinluyi F.O., Ojo B.T. Oyedele A.A., Bamisaye O.A., Olutomilola O.O., Magawata U.Z. 2021a. Resistivity Contrast and the Phenomenon of Geophysical Anomaly in Groundwater Exploration in A Crystalline Basement Environment, Southwestern Nigeria, International Journal of Earth Sciences Knowledge and Applications, 3 (1) 23-36

Bawallah M.A., Adiat K.A.N. Akinlalu A.A., Ilugbo S.O., Akinluyi F.O., Benjamin O.O., Oyedele AA., Omosuyi G.O, Aigbedion I. 2021b. Groundwater Sustainability and the Divergence of Rock Types in a Typical Crystalline Basement Complex Region, Southwestern Nigeria. Turkish Journal of Geosciences, 2(1), 1-11. DOI: 10.48053/turkgeo.777217

Bawallah M.A., Ilugbo S.O., Aina A.O., Olufemi B., Akinluyi F.O., Ojo B.T., Oyedele A.A., Olasunkanmi N.K. 2020a. Hydrogeophysical Studies of Central Kwara State Basement Complex of Nigeria. International Journal of Earth Sciences Knowledge and Application 2 (3) 146-164

Bawallah, M.A., Ofomola, M.O., Ilugbo, S.O. Aina, A.O., Olaogun, S.O., Olayiwola, K.O, Awoniran D.R., 2020b. Effect of Lineament and drainage orientation on groundwater potential of Moro Area Central Kwara State Nigeria. Indian Journal of Science and Technology 13 (10), 1124-1134.

Bawallah M.A., Adebayo A, Ilugbo S.O., Olufemi B., Alagbe O.A, Olasunkanmi K.N. 2018a. Evaluation of Groundwater Prospect in a Clay Dominated Environment of Central Kwara State, Southwestern Nigeria, International Journal of Advanced Engineering Research and Science, 5(6), 45-56

Bawallah M.A, Aina A.O., Ilugbo S.O., Ozegin K.O., Olasunkanmi K.N. 2018b. Evaluation of Groundwater Yield Capacity Using Dar-zarrouk Parameter of Central Kwara State, Southwestern Nigeria. Asian Journal of Geological Research, 1(1), 1-13

Djamel, B., 2017. Combining Resistivity and Aeromagnetic Geophysical Surveys for Groundwater Exploration in the Maghnia Plain of Algeria. Journal of Geological Research 1309053, 1-14.

Edet, A.E., and Okereke, C.S. (1996). Assessment of hydrogeological conditions in basement aquifers of the Precambrian Oban massif, southwestern Nigeria. Journal of Applied Geophysics, 36(1997), 195–204.

Ilugbo S.O., Adebiyi A.D. 2017. Intersection of Lineaments for groundwater prospect analysis using satellite remotely sensed and aeromagnetic dataset around Ibodi, Southwestern Nigeria. Int. J. of Phys Sci., 12(23), 329-353.

Ilugbo S.O., Ozegin K.O. 2018a. Significances of Deep Seated Lineament in Groundwater Studies around Ilesha, Southwestern Nigeria. Asian Journal of Geological Research, 1(1), 1-16,

Ilugbo, S.O., Adebiyi, A.D., Olomo, K.O., 2018b. Modeling of Groundwater Yield Using GIS and Electrical Resistivity Method in a Basement Complex Terrain, Southwestern Nigeria. Journal of Geography, Environment and Earth Science International 16 (1), 1-17.

Ilugbo S.O, Adebo B.A, Olomo K.O., Adebiyi A.D. 2018c. Application of Gis and Multi Criteria Decision Analysis to Geoelectric Parameters for Modeling of Groundwater Potential around Ilesha, Southwestern Nigeria. European Journal of Academic Essays 5(5), 105-123.

Ilugbo, S.O., Edunjobi, H.O., Alabi, T.O., Ogabi, A.F., Olomo, K.O., Ojo, O.A., Adeleke, K.A., 2019. Evaluation of Groundwater Level Using Combined Electrical Resistivity Log with Gamma (Elgg) around Ikeja, Lagos State, Southwestern Nigeria. Asian Journal of Geological Research 2(3), 1-13.

Ilugbo S. O., Adewoye O. E., Aladeboyeje A. I., Magawata U. Z., Oyedele A. A., Alabi T. O., Owolabi D. T., Adeleke K. A. and Adebayo S. O (2020a). Modeling of groundwater potential using remotely sensed data within Akure metropolis, Ondo State, Southwestern Nigeria, Applied Journal of Physical Science, Vol. 2(3), 38-54. https://doi.org/10.31248/AJPS2019.028

Ilugbo S.O., Edunjobi H.O., Adewoye O.E., Alabi T.O., Aladeboyeje A.I., Olutomilola O.O., Owolabi D.T. 2020b. Structural Analysis Using Integrated Aeromagnetic Data and Landsat Imagery in a Basement Complex Terrain, Southwestern Nigeria. Asian Journal of Geological Research, 3(2): 17-33

Joel E.S., Olasehinde P.I., De D.K., Maxwell O. 2016. Regional Groundwater Studies Using Aeromagnetic Technique. AAPG/SEG International Conference & Exhibition, Cancun, Mexico, September 6-9

Kardi, T. (2006). Analytic Hierarch Process (AHP) Tutorial http://people.revoledu.com/kardi/tutorial/ahp/ (accessed on the 10th June, 2009).

Kazeem O.O, Oluwatoyin K.O., Temitayo O.A., Jonathan I.I., Stephen O.I. 2022. Assessment of Groundwater Potential and Aquifer Vulnerabiliy Using Mcda and Drastic Analysis Within Akure Metropolis, Southwestern Nigeria. Big Data in Water Resources Engineering, 3(1): 15-20. http://doi.org/10.26480/bdwre.01.2022.15.20

Malczewski, J. (1999). GIS and Multicriteria decision analysis.pp 177–192, published by: John Wiley and Sons, Inc. United States of America.

Megwara JU, Udensi EE. Lineaments study using aeromagnetic data over parts of southern Bida basin, Nigeria and the surrounding basement rocks. International Journal of Basic and Applied Sciences. 2013;2(1):115-124.

Ndatuwong G., Yadav G.S. 2014. Integration of hydrogeological factors for identification of groundwater potential zones using remote sensing and GIS techniques. J Geosci Geomat 2(1):1–16. https :// doi.org/10.12691 /jgg-2-1-2

Ndikilar, C.E., Idi, B.Y., Terhemba, B.S., Idowu, I.I., Abdullahi, S.S., 2019. Applications of Aeromagnetic and Electrical Resistivity Data for Mapping Spatial Distribution of Groundwater Potentials of Dutse, Jigawa State, Nigeria. Modern Applied Science 13 (2), 11-20.

Ogunmola, J.K., Ayolabi, E.A., Olobaniyi, S.B. 2014. Lineament extraction from Spot 5 and Nigeria Sat-X imagery of the Upper Benue Trough, Nigeria‖, International Archives of the Photogrammetry, Remote Sensing and Spatial Information Sciences, Volume XL-1, ISPRS Technical Commission I Symposium, 17 – 20, Denver, Colorado, USA. pp. 323 330.

Oladejo, O.P., Sunmonu, L.A., Adagunodo, T.A. 2015. Groundwater Prospect in a Typical Precambrian Basement Complex Using Karous-Hjelt And Fraser Filtering Techniques. J.

Olorunfemi M.O. 2008. Voyage on the skin of the earth: a geophysical experience. Inaugural lecture series 211. Obafemi Awolowo University, Ife

Olorunfemi M.O., Oni A.G. 2019 Integrated geophysical methods and techniques for siting productive boreholes in basement complex terrain of Southwestern Nigeria. Ife J Sci 21(1):013–025. https :// doi.org/10.4314/ijsv2 1i1.2

Olorunfemi M.O., Oni A.G., Bamidele O.E., Fadare T.K., Aniko O.O. 2020. Combined geophysical investigations of the characteristics of a regional fault zone for groundwater development in a basement complex terrain of South-west Nigeria. SN Appl Sci 2:1033. https ://doi.org/10.1007/s4245 2-020-2363-6

Ojo J.S., Olorunfemi M.O., Akintorinwa O.J., Bayode S., Omosuyi G.O., Akinluyi F.O. (2015) GIS integrated geomorphological, geological and geoelectrical assessment of the groundwater potential of Akure Metropolis, southwest Nigeria. J Earth Sci Geotech Eng 5(14):85–101

Oyedele A.A.2019. Use of remote sensing and GIS techniques for groundwater exploration in the basement complex terrain of Ado-Ekiti, SW Nigeria. Appl Water Sci 9(51):1–13. https ://doi.org/10.1007/s1320 1-019-0917-9

Palacky, G.J., Ritsema, I.L., and De Jong, S.J. (1981). Electromagnetic prospecting for groundwater in pre-cambrian terrains in the republic of Upper Volta (Burkina Faso). Geophysical prospecting, vol. 31, pp 932 – 955.

Pietersen, K., 2006. Multiple criteria decision analysis (MCDA): A tool to support sustainable management of groundwater resources in South Africa. Water SA 32 (2), 119-128

Rahaman, M.A. 1976. Review of the basement of S.W. NigeriaInc. Kogbe (ed) Geology of Nigeria. Elizabethan press, Lagos, 41 – 58.

Rao, B.V., and Briz-Kishore, B.H. (1991). A methodology for locating potential aquifers in a typical semi-arid region in India using resistivity and hydrogeologic parameters. Geoexploration, 27, 55-64.

Saaty TL (2008) Decision making with the analytic hierarchy process. Int J Serv Sci 1(1):83. https ://doi.org/10.1504/IJSSC I.2008.017590

Shailaja G., Kadam A.K., Gupta G., Umrikar B.N., Pawar N.J. (2018). Integrated geophysical, geospatial and multiple-criteria decision analysis techniques for delineation of groundwater potential zones in a semi-arid hard-rock aquifer in Maharashtra, India. Hydrogeol J 5:545. https ://doi.org/10.1007/s1004 0-018-1883-2

Singh P, Thakur JK, Kumar S (2013) Delineating groundwater potential zones in a hard-rock terrain using geospatial tools. Hydrol Sci J 58(1):213–223. https ://doi.org/10.1080/02626 667.2012.74564 4

Tolche AD (2020) Groundwater potential mapping using geospatial techniques: a case study of Dhungeta-Ramis sub-basin. Ethiopia Geol Ecol Landsc. https ://doi.org/10.1080/24749 508.2020.1728882

Telford, W.M., Geldart, L.P., Sheriff, R.E. and Keys, D.A. (1990): Applied geophysics, 2nd Edn., Cambridge University Press.

Talabi, A. O., Tijani, M.N. 2011. Integrated remote sensing and GIS approach to groundwater potential assessment in the basement terrain of Ekiti area southwestern Nigeria. RMZ Mater Geoenviron, 58(3), 303-328.

Waikar, M. L., Aditya, P. N. 2014. Identification of groundwater potential zone using remote sensing and GIS technique. *International Journal of Innovative Research in Science,* Engineering and Technology*,* 3(5), 12163-12174

Table 5

Table 5 is not available with this version.

Figures

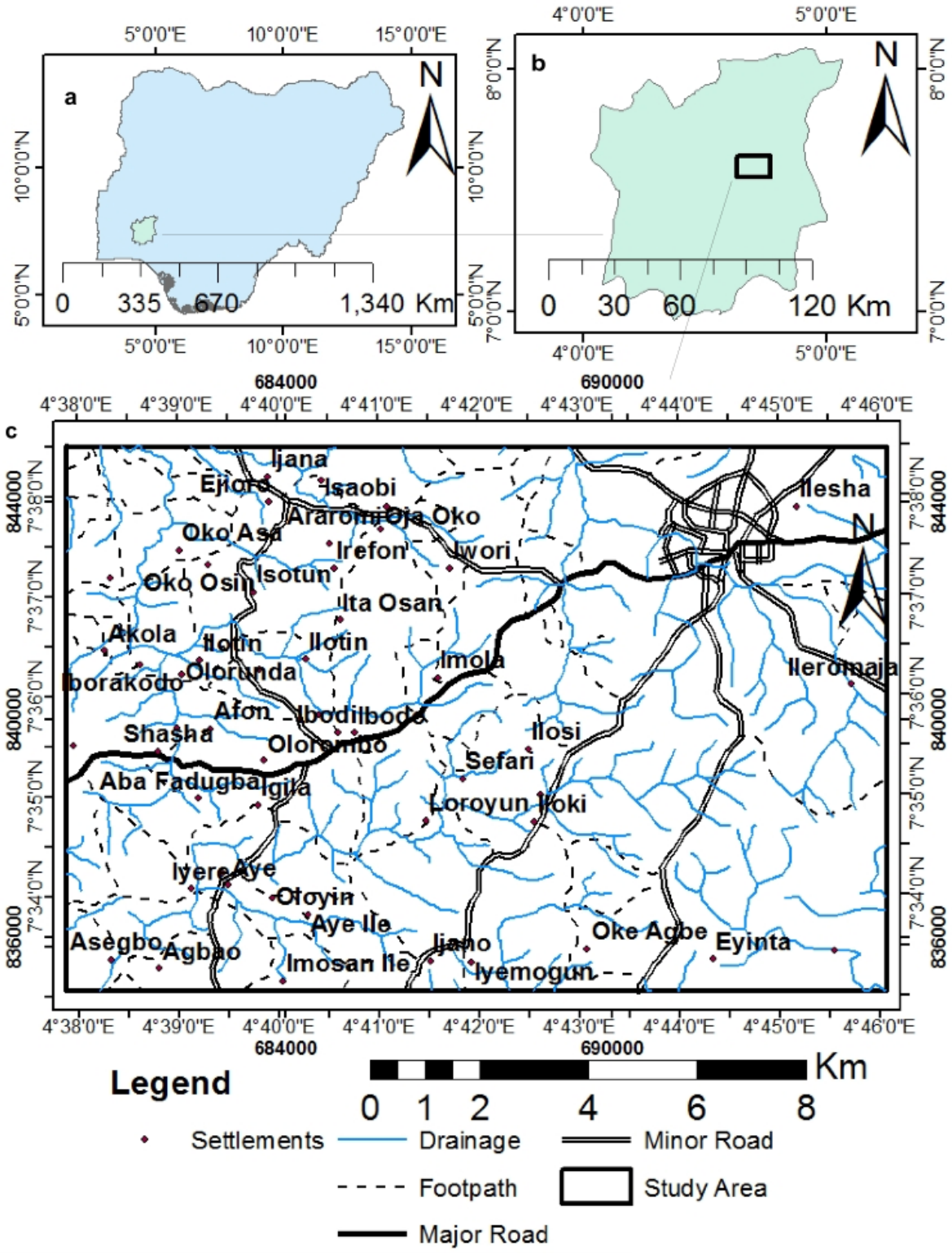

Figure 1

(a) Map of Nigeria and Osun State, (b) Map of Osun State Showing the Study Area (c) Location Map of Ilesha and its Environ (after Topographic Map of Ilesha SW sheet 234, 1965)

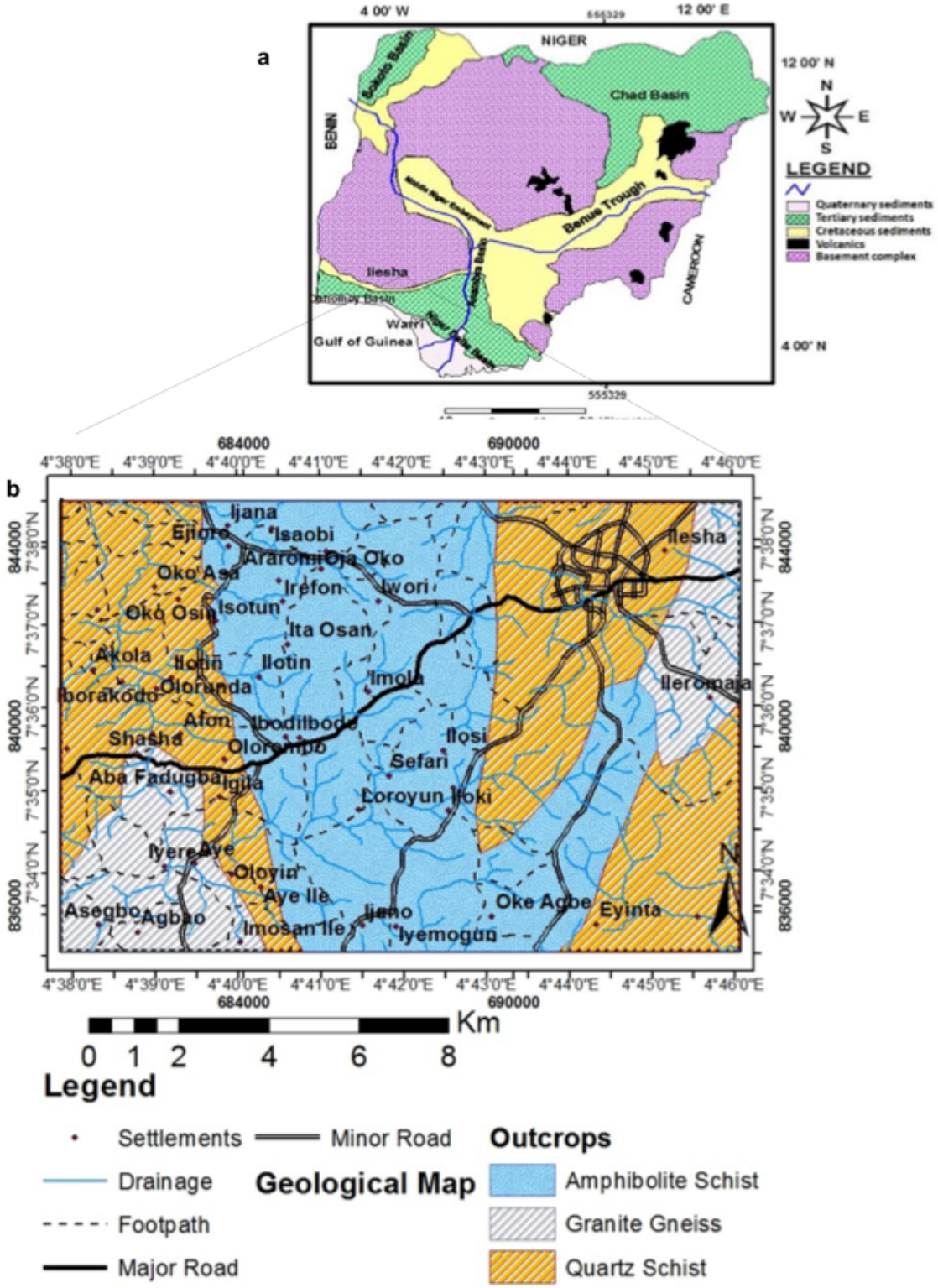

Figure 2

(a) Geological Map of Nigeria (b) Geological Map of the Study Area

(after Geological Survey of Ilesha Iwo Schist 60, 1980)

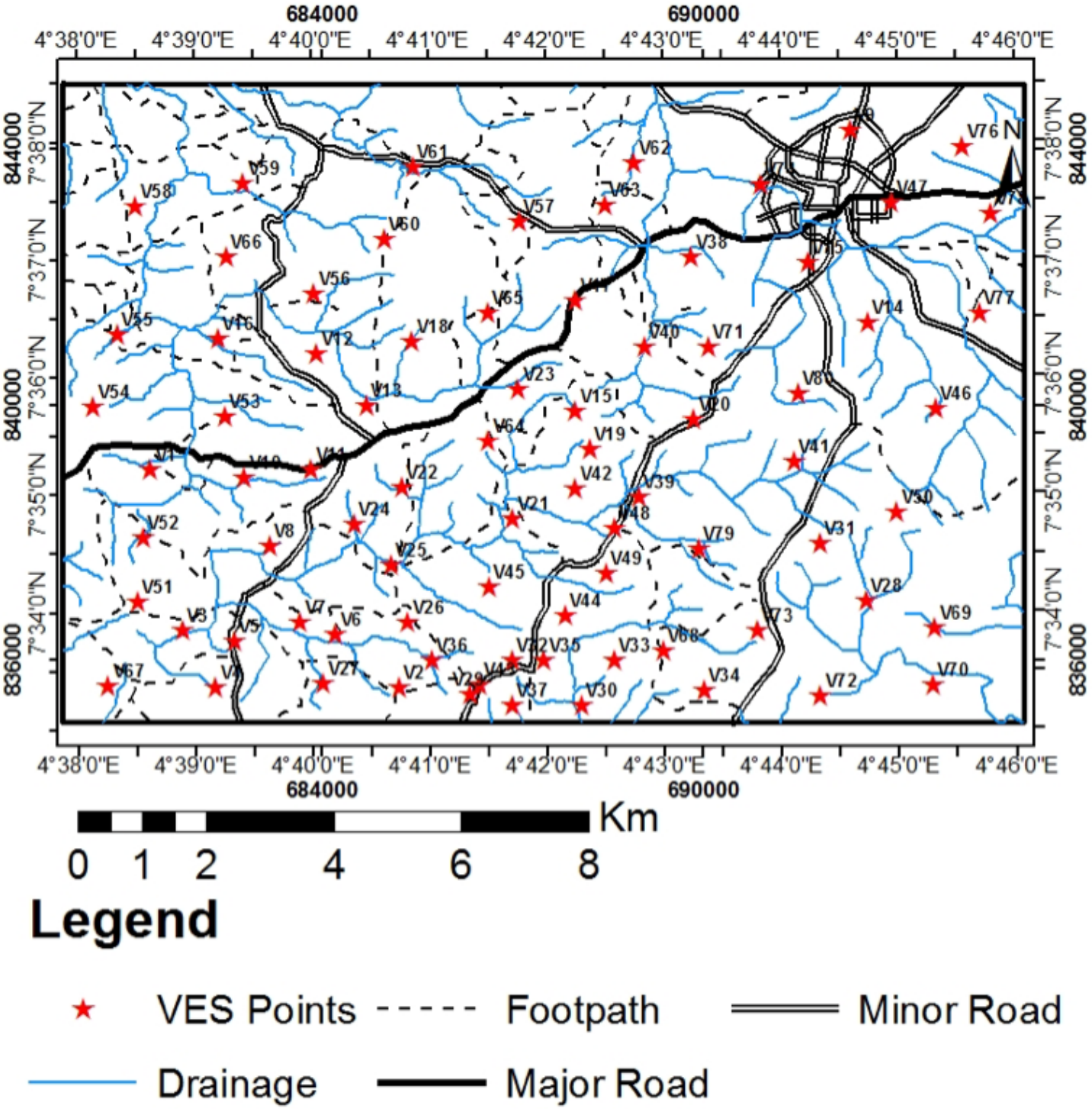

Figure 3

VES Data Points Map of the Study Area..

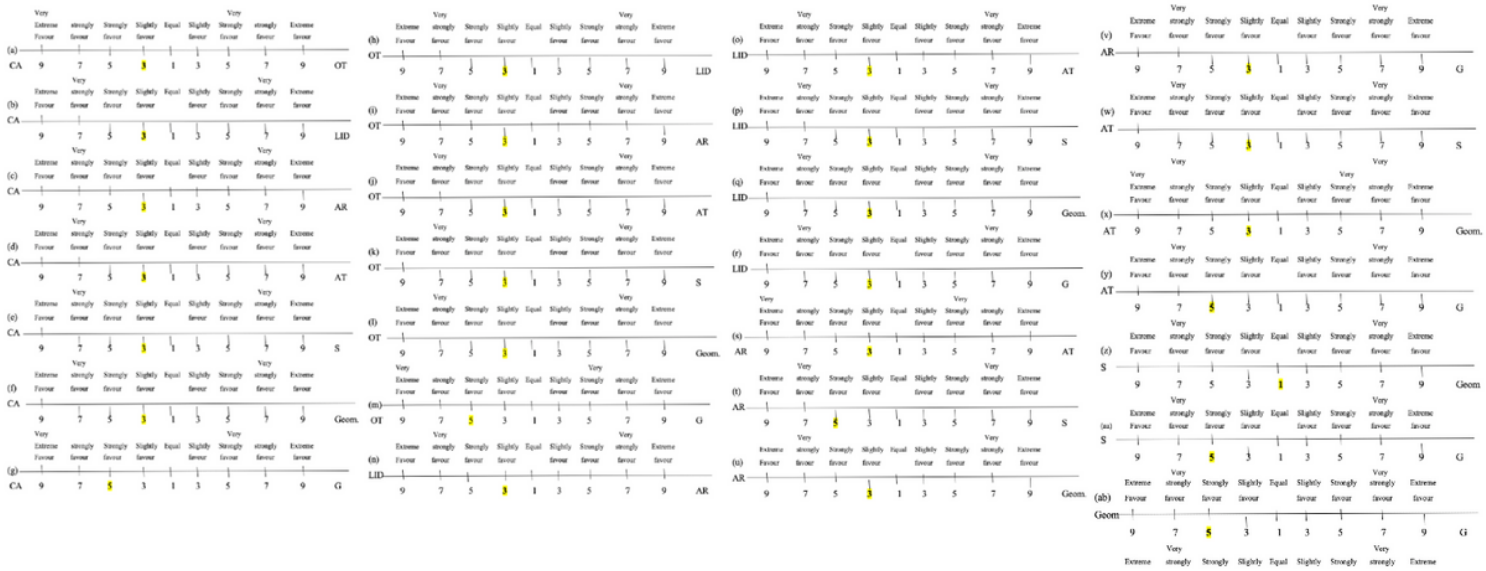

Figure 4

(a-ab): Pairwise comparisons of the criteria/parameter for Groundwater Potential (modified after kardi, 2006, Adiat *et al.,* 2013)

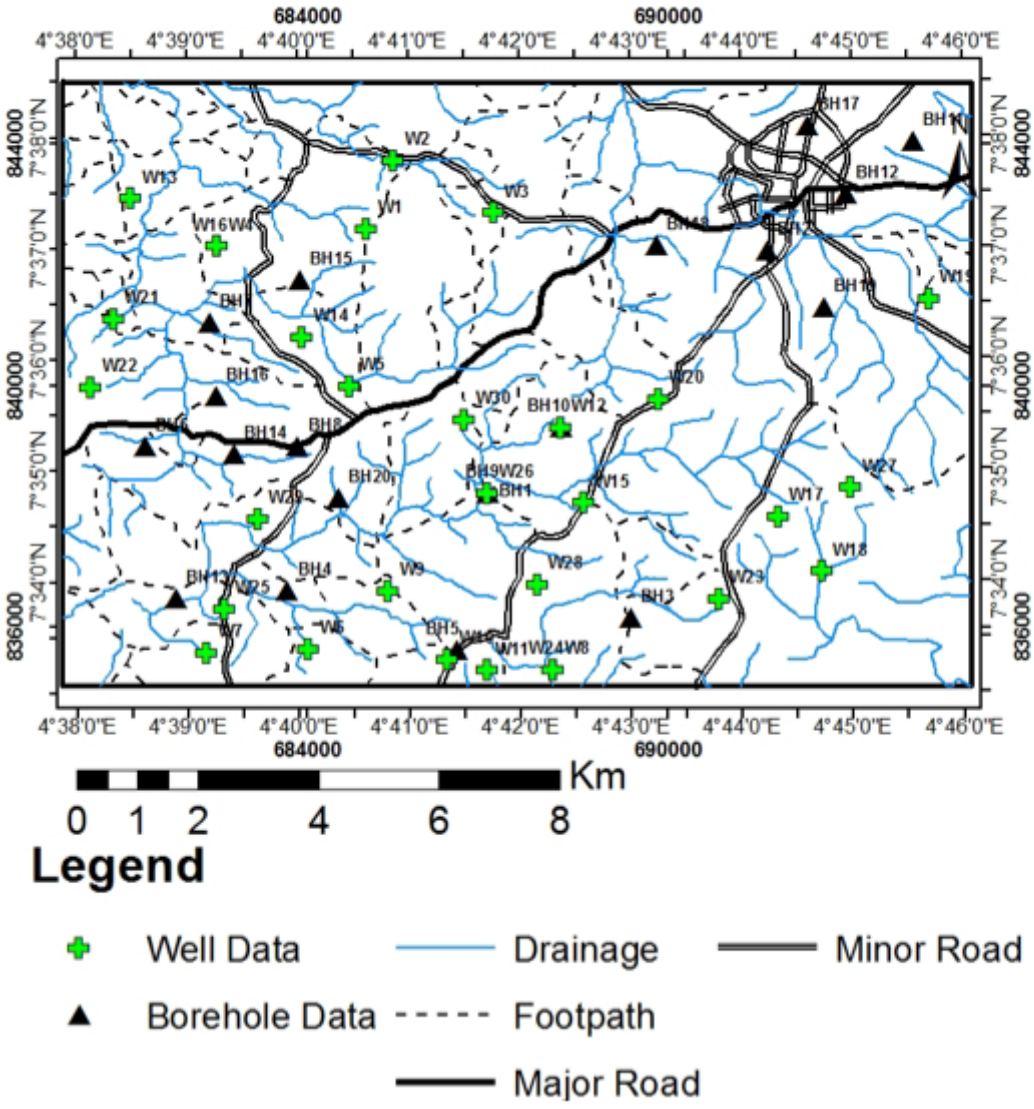

Figure 5

Data Acquisition Map of the Study Area Showing the Borehole Data and Static Water Level

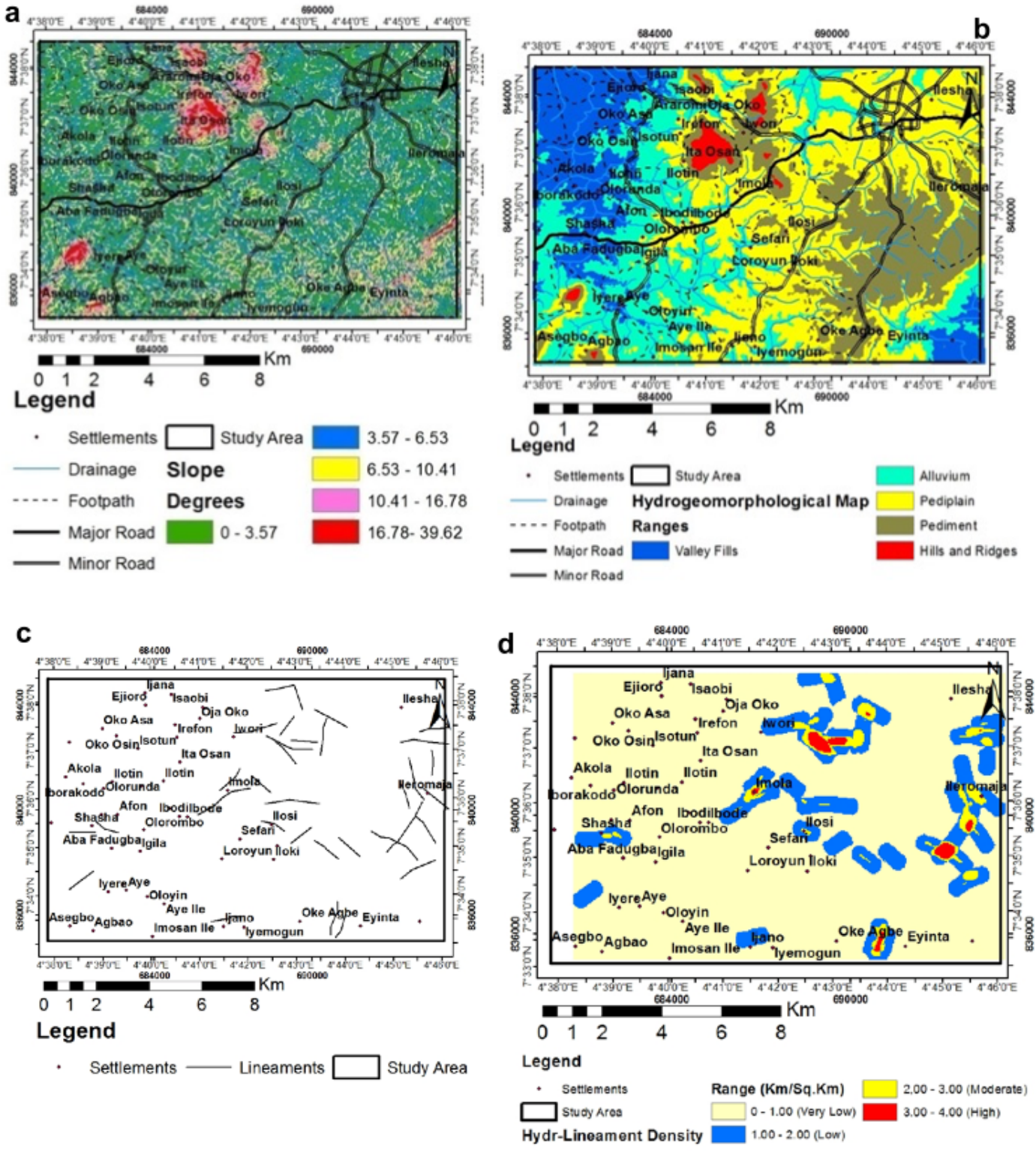

Figure 6

(a) Slope map (b) Geomorphological Map (c) Lineament Map (d) Lineament Density of the Study Area

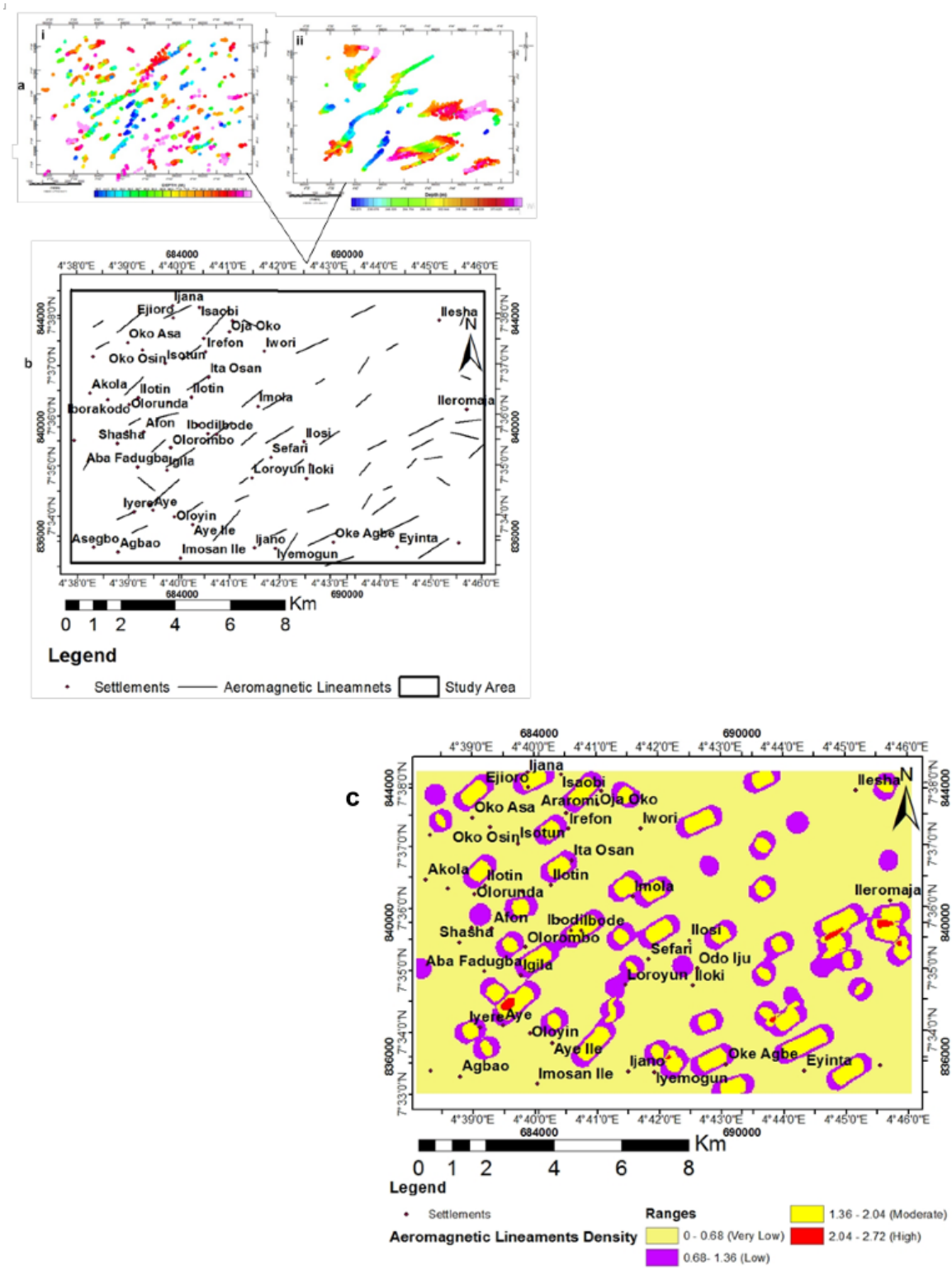

Figure 7

(a) 3D Euler Solution from the Analysis of Aeromagnetic Data with Structural Index (i = 1.0 and ii = 2.0)
(b) Lineaments Map (c) Aeromagnetic Lineaments Density Map of the Study Area

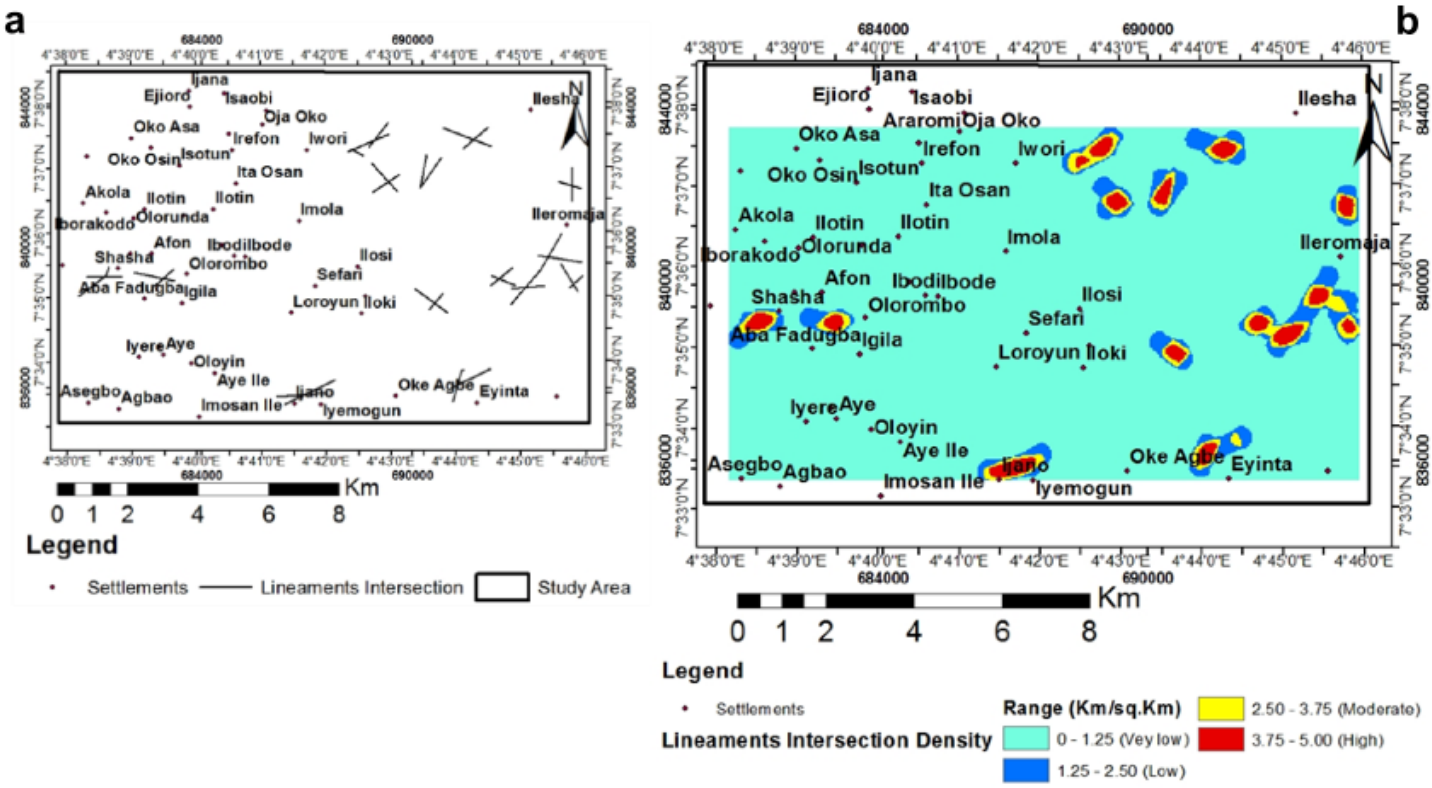

Figure 8

(a) Lineaments Intersection Map (b) Lineament Intersection Density Map of the Study Area

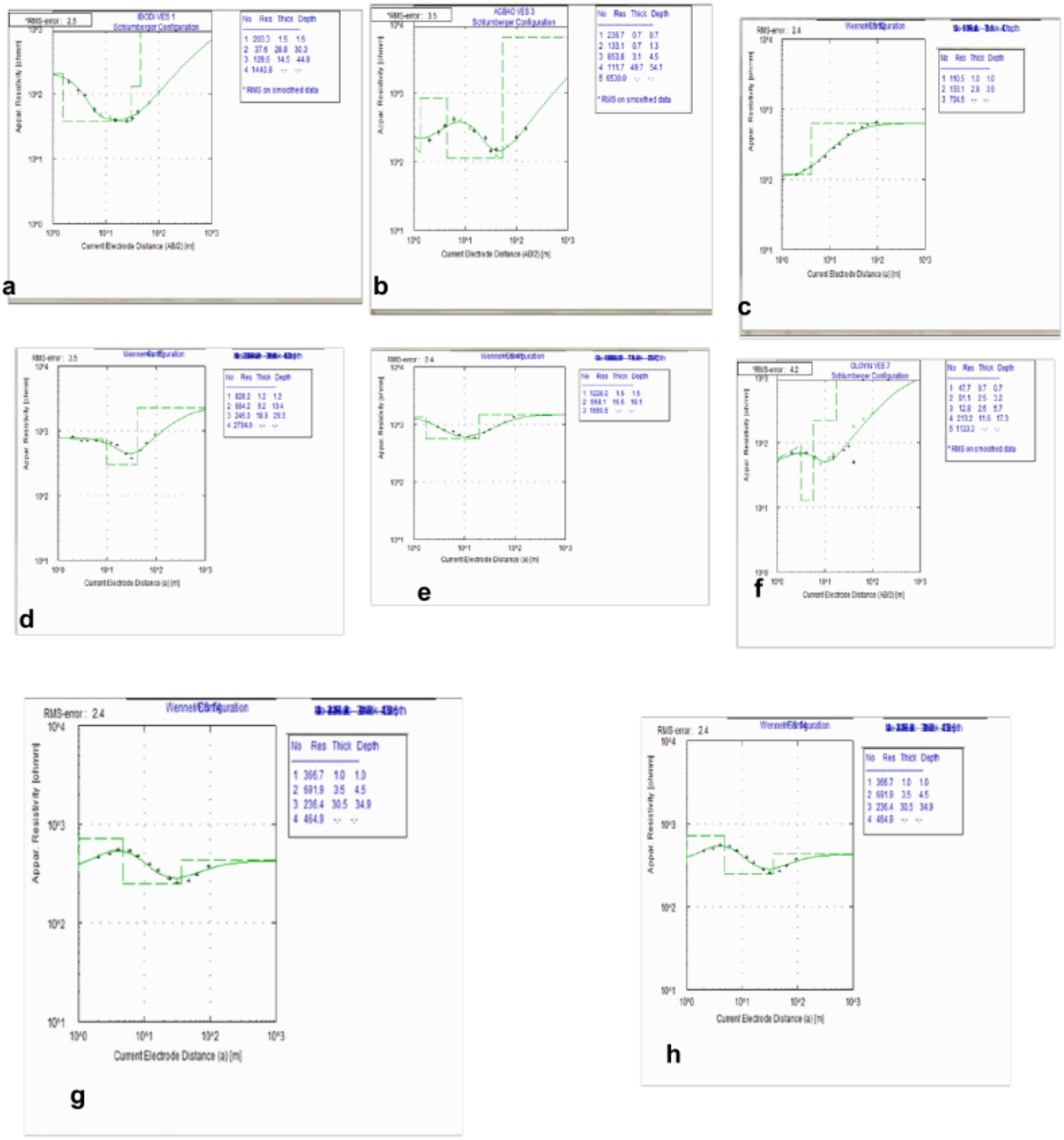

Figure 9

Showing Typical Curve Types (a) HA (b) HKH (c) A (d) QH (e) H (f) KHA (g) KQH (h) KH

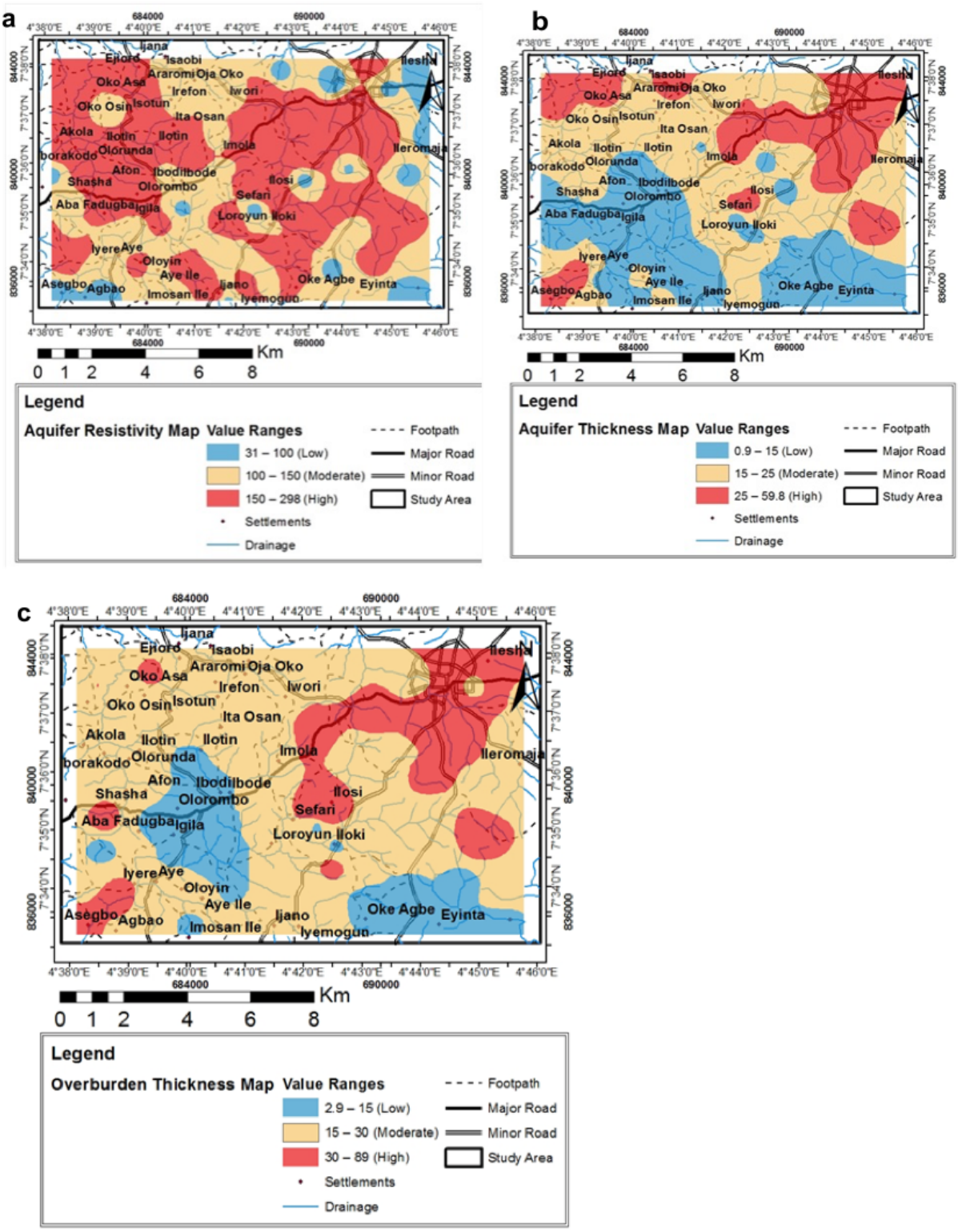

Figure 10

(a) Aquifer Resistivity Map (b) Aquifer Thickness Map (c) Overburden Thickness of the Study Area

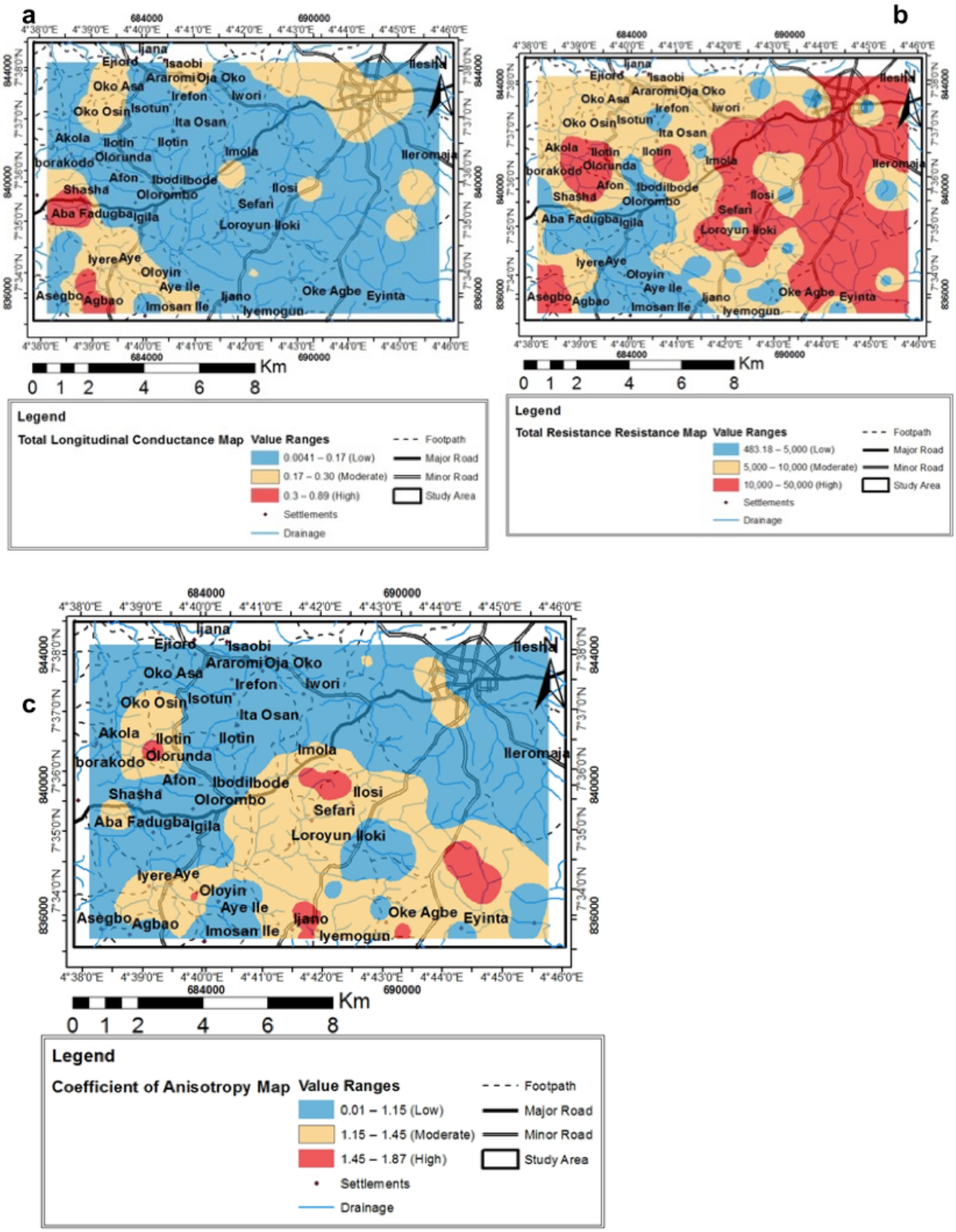

Figure 11

(a) Total Longitudinal Conductance Map (b) Total Transverse Resistance Map (c) Coefficient of Anisotropy Map of the Study Area

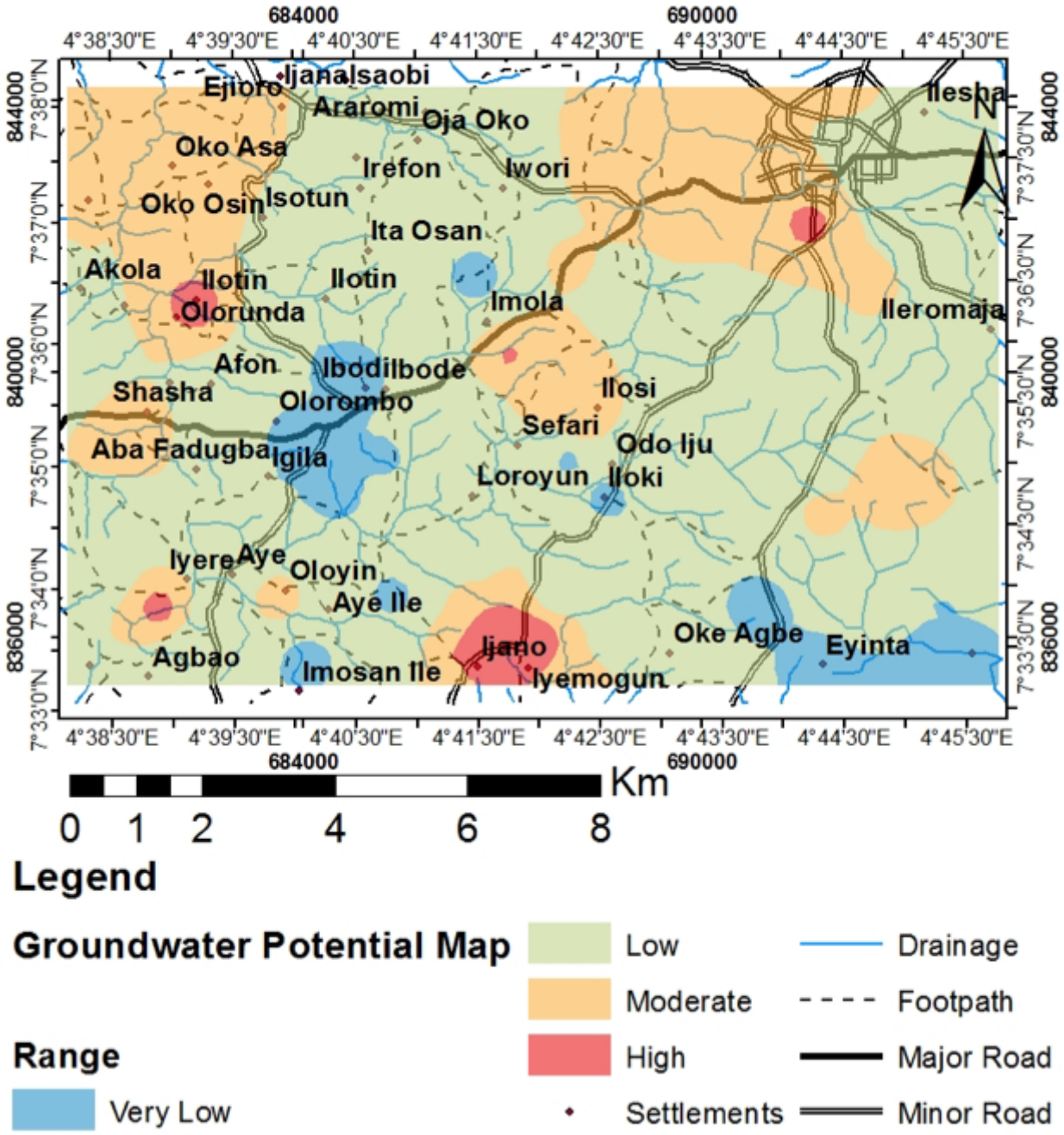

Figure 12

Groundwater Potential Map of the Study Area

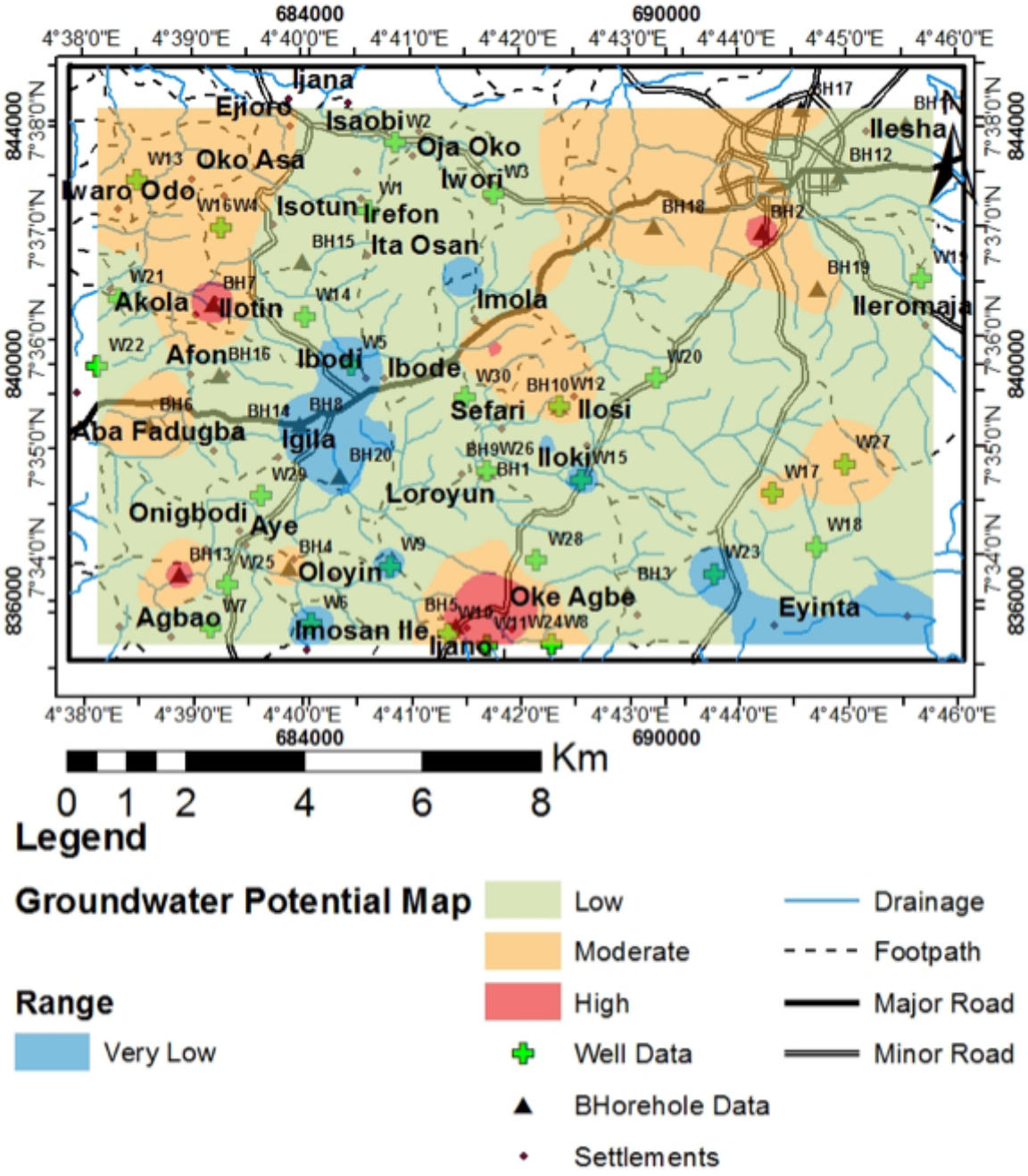

Figure 13

Validation Map of the Study Area